

Analytic mode matching for a circular dissipative silencer
containing mean flow and a perforated pipe

Ray Kirby

School of Engineering and Design,

Mechanical Engineering,

Brunel University, Uxbridge, Middlesex, UB8 3PH, UK.

Francisco D. Denia

Departamento de Ingeniería Mecánica y de Materiales,

Universidad Politécnica de Valencia,

Camino de Vera s/n, 46022 Valencia, Spain

ABSTRACT

An analytic mode matching scheme that includes higher order modes is developed for a straight-through circular dissipative silencer. Uniform mean flow is added to the central airway and a concentric perforated screen separates the mean flow from a bulk reacting porous material. Transmission loss predictions are compared with experimental measurements and good agreement is demonstrated for three different silencers. Furthermore, it is demonstrated that, when mean flow is present, the axial kinematic matching condition should equate to that chosen for the radial kinematic boundary condition over the interface between the airway and the material. Accordingly, if the radial matching conditions are continuity of pressure and displacement, then the axial matching conditions should also be continuity of pressure and displacement, rather than pressure and velocity as previously thought. When a perforated screen is present the radial pressure condition changes, but the radial kinematic condition should always remain equivalent to that chosen for the axial kinematic matching condition; here, results indicate that continuity of displacement should be retained when a perforated screen is present.

I. INTRODUCTION

Dissipative silencers are often used to attenuate broadband noise emanating from fluid moving devices such as fans and internal combustion engines. When the velocity of the mean gas flow generated by a device is high, relative to the ambient speed of sound, then the acoustic performance of a dissipative silencer may be altered significantly when compared to that found in the absence of mean flow. Automotive dissipative silencers are often required to perform in environments in which the mean flow Mach number reaches values of up to 0.2; under such circumstances the effect of the mean flow should be accounted for when measuring and/or predicting silencer performance. Accordingly, this paper investigates the effect of mean flow on the acoustic performance of a typical “straight-through” bulk reacting dissipative silencer that contains a perforated screen separating the mean gas flow from the absorbing material. Theoretical predictions are obtained using an analytic approach that assumes a uniform and incompressible mean gas flow, and predictions are compared with experimental measurement and the finite element method.

Mean flow has long been known to affect dissipative silencer performance, although relatively few studies take this into account. Early work on automotive dissipative silencers focussed on predicting modal attenuation in infinite silencers; for example, Nilsson and Brander¹, and later Cummings and Chang² obtained a number of eigenmodes for a circular silencer when mean flow was present in the central airway. Here, roots of the governing eigenequation were found using an appropriate analytic¹ or numerical root finding technique². Nilsson and Brander¹ also included a perforated screen in their model, although later work on discontinuities (with potential

for application to silencers of finite length) relied in the Wiener-Hopf technique, which is, arguably, a complex and difficult method to generalise for dissipative silencers. Cummings and Chang² omitted a perforated screen but added mean flow in the liner itself, on the basis that axial static pressure drops generated at the interface between the airway and the material induced a mean flow in the material. It is unlikely, however, that these effects will be relevant when a perforated screen is present, as the screen will significantly reduce frictional effects at the interface between the airway and the material and so reduce the axial static pressure gradient over the silencer section. An alternative method was proposed by Astley and Cummings³ who used finite elements to compute the silencer eigenmodes for a general cross-section, although they omitted a perforated screen from the analysis. A finite element based method has the advantage that it does not rely on root finding techniques (that are known to be susceptible to missing modes) in order to find the required eigenmodes for the silencer, although this is normally at the expense of extra computational effort.

Dissipative silencer models that are based on modal attenuation alone are of limited use for predicting overall silencer performance as they neglect sound scattering over the inlet and outlet planes of the silencer. Moreover, measurements of silencer performance are normally reported in terms of the sound power difference across the (finite length) silencer. In view of this, Cummings and Chang⁴ used the silencer eigenmodes in an analytic mode matching scheme that enforced continuity of pressure and axial velocity over the inlet and outlet planes of the silencer. Sound power reduction across the silencer (the silencer transmission loss) was then calculated for mean flow mach numbers of up to 0.196. This method depends on finding a sufficient number of eigenmodes to generate a converged solution: for silencers of a relatively modest size,

Cummings and Chang found that up to six modes were necessary. A fast and efficient alternative to Cummings and Chang's method was proposed by Peat⁵, and later by Kirby⁶, who both developed closed form analytic solutions based on the attenuation of the fundamental mode only. Kirby⁶ included a perforated screen and, by adding extra terms to the series expansions of the Bessel and Neumann functions, achieved a more accurate model when compared to that proposed by Peat⁵. The methods of Peat⁵ and Kirby⁶ are, however, accurate only over a limited frequency range for a given silencer geometry and/or material parameters. Such limitations apply also to other methods based on the fundamental mode, for example those methods investigated by Panigrahi and Munjal⁷.

An alternative approach for predicting the transmission loss of dissipative silencers with mean flow is the finite element based method of Peat and Rathi⁸. Here, mean flow is included in the central airway, but a three dimensional induced flow field is also introduced into the liner. This approach extends the one dimensional assumed flow field of Cummings and Chang⁴, and is also capable of modelling silencers of arbitrary shape (provided the geometry of the central airway is uniform). In common with Cummings and Chang, Peat and Rathi omitted a perforated screen, although when the two methods were compared agreement between them was poor at low frequencies. Peat and Rathi were, rightly, surprised by this and they tentatively proposed that these discrepancies in the transmission loss predictions were caused by the use of differing material parameters. One disadvantage of Peat and Rathi's method is that it is time consuming to implement, as it is based on the finite element method and in order to find the silencer four poles one must solve the problem twice, using two different axial boundary conditions. For a uniform dissipative silencer (of arbitrary cross-section), Kirby⁹ proposed using a point

collocation technique that is, essentially, a numerical mode matching method. This reduces the dimensions of the problem by one and so speeds up solution time, although this method is still based on the finite element method. Kirby⁹ also added a perforated screen to his model and neglected an induced mean flow field in the liner; predictions were presented for two elliptical dissipative silencers and good agreement with experiment was reported.

In general it is desirable to include higher order modes in any predictive scheme for dissipative silencers. Moreover, when mean flow is present a perforate screen is almost always used to reduce static pressure losses over the silencer and to prevent egress of the lining material. To date, the only approach in the literature that accommodates mean flow, a bulk reacting absorbent, and a perforated screen is the point collocation method of Kirby⁹. However, this approach depends on the use of the finite element method and the writing of dedicated finite element software, which is not always the favoured option for researchers. Furthermore, Kirby's method⁹ is similar to Cumming and Chang's method⁴ in that it uses a modal expansion to represent the sound field in the silencer, and then matches acoustic pressure and axial velocity over the inlet and outlet planes of the silencer. Problems with Cummings and Chang's⁴ mode matching predictions were noted by Peat and Rathi⁸ and, although Kirby⁹ reported good agreement between prediction and experiment, those problems with Cummings and Chang's method have yet to be resolved. Therefore, until these problems have been addressed, mode matching cannot yet be considered fully validated when mean flow is present, and this is true also for the numerical matching scheme of Kirby⁹. Accordingly, this paper intends to review the appropriate axial matching conditions when mean flow is present and this is most readily achieved using an analytic mode matching approach based on Cummings and Chang's method⁴. Moreover,

although this approach requires solutions to be found for the governing silencer eigenequation, analytic methods are also popular for the ease in which computer code can be written and applied. Evidence for this latter point may be found in the large number of recent articles that rely on analytic mode matching in order to study the effect of a perforated screen on dissipative silencers without mean flow; see, for example, Refs. 10 and 11. This article will extend this work to include mean flow.

This work begins by obtaining the eigenmodes in the silencer chamber and the inlet/outlet pipes. Here, the appropriate radial matching conditions for a perforated screen subjected to grazing mean flow and backed by a porous material are discussed and a root finding technique is also discussed in detail. The appropriate axial matching conditions over the inlet/outlet planes of the silencer are then reviewed and conclusions drawn after comparing predictions with the finite element calculations of Peat and Rathi⁸ in the absence of a perforated screen, and with point collocation predictions generated using the method of Kirby⁹. Finally, a comparison is made between the new analytic mode matching method and experimental measurements for three different silencers with mean flow Mach numbers of 0.15, and two impedance models for the perforated screen are also investigated.

II. THEORY

The dissipative silencer is assumed to have a uniform circular cross-section and to contain a uniform mean gas flow of Mach number M in the central channel (see Fig. 1). In the silencer chamber a perforate screen separates the central channel (region 2) from a bulk reacting (isotropic) porous absorbent (region 3). A plane wave propagates in the positive x direction in region 1, and the outlet pipe (region 4) is terminated anechoically. The pipe walls in regions 1 and 4, and the walls of the silencer chamber, are assumed to be rigid and impervious to sound. The analysis proceeds by assuming that the acoustic fields in the inlet/outlet pipes, and also the silencer chamber, may be expanded as an infinite sum over the pipe/silencer eigenmodes. On finding the pipe/silencer eigenfunctions and associated wavenumbers, the modal amplitudes are computed by matching analytically over the two axial discontinuities, after suitable truncation of each modal sum.

A. Sound field in the inlet/outlet pipes.

The acoustic wave equation in region 1 (or region 4, which is identical) is given by

$$\frac{1}{c_0^2} \frac{D^2 p_1'}{Dt^2} - \nabla^2 p_1' = 0, \quad (1)$$

where c_0 is the isentropic speed of sound in air, p_1' is the acoustic pressure and t is time. For an axisymmetric silencer, and assuming a time dependence of $e^{i\omega t}$ (where $i = \sqrt{-1}$ and ω is the radian frequency), equation (1) may be re-written as

$$(1-M^2)\frac{\partial^2 p'_1}{\partial x^2} + \frac{1}{r}\frac{\partial p'_1}{\partial r} + \frac{\partial^2 p'_1}{\partial r^2} - 2iMk_0\frac{\partial p'_1}{\partial x} + k_0^2 p'_1 = 0, \quad (2)$$

where $k_0 = \omega/c_0$ and M is the mean flow Mach number. The sound pressure is now written as an expansion over the pipe eigenmodes to give

$$p'_1(x, r) = \sum_{n=0}^{\infty} F^n \Phi_i^n(r) e^{-ik_0 \lambda_i^n x} + \sum_{n=0}^{\infty} A^n \Phi_r^n(r) e^{-ik_0 \lambda_r^n x}, \quad (3)$$

and

$$p'_4(x', r) = \sum_{n=0}^{\infty} D^n \Phi_i^n(r) e^{-ik_0 \lambda_i^n x'} + \sum_{n=0}^{\infty} E^n \Phi_r^n(r) e^{-ik_0 \lambda_r^n x'}. \quad (4)$$

Here, F^n , A^n , D^n , and E^n are the modal amplitudes, λ_i^n are the incident and λ_r^n the reflected axial wavenumbers, and Φ_i^n are the incident and Φ_r^n the reflected eigenfunctions, in regions 1 and 4 respectively. The wavenumbers and eigenfunctions for the incident and reflected sound fields are found by substituting equations (3) and (4) into equation (2). For the axial wavenumbers, this yields

$$\lambda_{i,r}^n = \left\{ -M \mp \sqrt{1 - (1-M^2) \left[\frac{a_1^n}{k_0 r_1} \right]^2} \right\} / (1-M^2). \quad (5)$$

Here, the incident wave is calculated using the minus, and the reflected wave using the plus, before the square root; r_1 is the radius of the pipe in region 1, and a_1^n are solutions of the rigid

wall boundary condition $J_1(a_1) = 0$ (J_m is a Bessel function of the first kind and order m). The eigenfunctions are given as

$$\Phi_{i,r}^n(r) = J_0(\gamma_{i,r}^n r), \quad (6)$$

where $\gamma_{i,r}$ is a radial wavenumber given by $\gamma_{i,r}^n = a_1^n / r_1$.

B. Sound field in the chamber.

The acoustic wave equation in region 2 is given by equation (2). For region 3, the acoustic wave equation may be written [6] as

$$\frac{\partial^2 p'_3}{\partial x^2} + \frac{1}{r} \frac{\partial p'_3}{\partial r} + \frac{\partial^2 p'_3}{\partial r^2} - \Gamma^2 p'_3 = 0, \quad (7)$$

where Γ is the propagation constant for the porous material. The sound pressure fields in regions 2 and 3 are coupled and written as an expansion over the chamber eigenmodes to give

$$p'_c(x, r) = \sum_{n=0}^{\infty} B^n \Psi_i^n(r) e^{-ik_0 k_i^n x} + \sum_{n=0}^{\infty} C^n \Psi_r^n(r) e^{-ik_0 k_r^n x}. \quad (8)$$

Here, B^n and C^n are the modal amplitudes, k_i^n are the incident and k_r^n the reflected axial wavenumbers, and Ψ_i^n are the incident and Ψ_r^n the reflected eigenfunctions. The substitution of equation (8) into equations (2) and (7) allows the radial pressure for a positive travelling wave and for eigenmode n , to be written as

$$p'_{2_i}(r) = P_2^n J_0(\alpha_i^n r) \quad (9)$$

and

$$P'_{3_i}(r) = P_{3_i}^n \left[J_0(\beta_i^n r) - \frac{Y_0(\beta_i^n r) J_1(\beta_i^n r_2)}{Y_1(\beta_i^n r_2)} \right]. \quad (10)$$

Here, two identical expressions may also be written for a reflected wave. The terms $P_{2_{i,r}}^n$ and $P_{3_{i,r}}^n$ are constants, r_2 is the radius of the silencer chamber and Y_m denotes a Neumann function of order m . The radial wavenumbers α and β are given by

$$\alpha_{i,r}^n = k_0 \sqrt{1 - 2Mk_{i,r}^n - (1 - M^2)(k_{i,r}^n)^2}, \quad (11)$$

and

$$\beta_{i,r}^n = k_0 \sqrt{-\tilde{\Gamma}^2 - (k_{i,r}^n)^2}, \quad (12)$$

where $\tilde{\Gamma} = \Gamma/k_0$. The eigenequation for the chamber is found by eliminating $P_{2_{i,r}}^n$ and $P_{3_{i,r}}^n$ from equations (9) and (10) using the appropriate radial boundary conditions over the perforated screen.

In the absence of a perforated screen the accepted (distributed) boundary conditions when uniform mean flow is present are continuity of pressure and displacement. However, when a perforated screen is present, identifying the correct distributed boundary conditions is more problematic because the screen is treated as an infinitely thin distributed boundary, whereas in reality experimental measurements are taken for a single (discrete) orifice of finite thickness¹². Moreover, when grazing mean flow is present, impedance measurements include the effects of a viscous boundary layer adjacent to one side of the perforated screen, whereas the model assumes an infinitely thin boundary layer. The pressure condition over the perforated screen is normally

written so that the change in pressure (Δp) over the perforated screen is expressed in terms of the measured impedance ζ and the acoustic velocity in the orifice U , to give $\Delta p = \zeta U$. The difficulty lies in identifying the second continuity condition and Kirby^{6,9} retained continuity of displacement, a decision based on the earlier work of Nilsson and Brander¹; however, this means that the choice of U is ambiguous when defining the pressure condition. Recently, Aurégan and Leroux¹³ used a discrete plane wave approach to model a reactive silencer and examined the second continuity condition under sheared grazing mean flow. They conclude that the correct condition lies somewhere between continuity of displacement and continuity of velocity. Dokumaci¹⁴ proposed using a “slip” velocity to accommodate the departure from an assumed no slip condition at the wall of the perforated screen, and also a term that accounts for the non-uniformity of the actual mean flow profile. Using a distributed model of the perforated screen, Dokumaci¹⁴ demonstrates the effect of these two parameters on transmission loss predictions for a straight through reactive silencer, although no comparisons were made with experimental measurements and so no conclusions regarding appropriate values for these parameters were forthcoming. Clearly, work on reactive silencers illustrates some difficulty in successfully identifying the appropriate second continuity condition for the perforated screen. Furthermore, the model presented here examines a dissipative silencer and also includes higher order modes, and so it is debatable whether the analysis for reactive silencers is directly applicable to the present case. Nevertheless, in view of the problems seen for reactive silencers the following condition (for eigenmode n , incident or reflected wave) over the perforated screen is specified,

$$\tilde{\rho} \left[1 - Mk^n \right]^{-T} \frac{\partial p'_2}{\partial r}(x, r_1) = \frac{\partial p'_3}{\partial r}(x, r_1). \quad (13)$$

Here T is a constant, where $1 \leq T \leq 2$; $T = 1$ corresponds to continuity of velocity, and $T = 2$ to continuity of displacement. The density of air in region 2 is denoted by ρ_0 and in region 3 the effective (complex) density is denoted by $\rho(\omega)$,⁶ where $\tilde{\rho} = \rho(\omega)/\rho_0$. The pressure condition over the perforated screen is written as

$$p'_2(x, r_1) - p'_3(x, r_1) = \rho_0 c_0 \zeta u'_{3r}(x, r_1), \quad (14)$$

where u'_{3r} is the radial acoustic velocity in region 3. Equation (14) is written in terms of the velocity in region 3, rather than region 2, in order to reflect the acoustic velocity used in the measurements of impedance under the influence of grazing mean flow, see for example Refs. 12 and 15. Thus, although theoretically the choice of velocity here is still ambiguous if one assumes $T = 2$, the discussions above suggest that it is appropriate always to choose the velocity used when measuring, and hence defining, the impedance.

Equations (13) and (14) are now combined with equations (9) and (10) to give the following eigenequation for the chamber (for eigenmode n , incident or reflected wave):

$$\left\{ [1 - Mk]^T \frac{J_0(\alpha r_1)}{J_1(\alpha r_1)} + \frac{i\zeta\alpha}{k_0} \right\} - \frac{\tilde{\rho}\alpha}{\beta} \left[\frac{J_1(\beta r_1)Y_1(\beta r_2) - Y_1(\beta r_1)J_1(\beta r_2)}{J_0(\beta r_1)Y_1(\beta r_2) - Y_0(\beta r_1)J_1(\beta r_2)} \right] = 0. \quad (15)$$

The transverse eigenfunction is given by

$$\Psi(r) = \left\{ \begin{array}{ll} J_0(\alpha r) & 0 \leq r \leq r_1 \\ \frac{\tilde{\rho}\alpha}{\beta} \frac{J_1(\alpha r_1)}{[1 - Mk]^T} \frac{[J_0(\beta r)Y_1(\beta r_2) - Y_0(\beta r)J_1(\beta r_2)]}{[J_1(\beta r_1)Y_1(\beta r_2) - Y_1(\beta r_1)J_1(\beta r_2)]} & r_1 \leq r \leq r_2 \end{array} \right\}. \quad (16)$$

The incident and reflected wavenumbers for the chamber $k_{i,r}^n$ are found by solving eigenequation (15). Here, the roots are found using the Newton Raphson method, which is discussed in detail in Appendix A.

C. Analytic mode matching.

The modal amplitudes in equations (3), (4) and (8) are found by enforcing matching conditions over the inlet ($x=0$) and the outlet ($x=L$) of the silencer. The appropriate axial matching conditions are continuity of pressure and a kinematic continuity condition that is written here in terms of the constant T , specified in equation (13). Accordingly, continuity of pressure over planes A and B yields

$$p_1'(0, r) = p_2'(0, r), \quad 0 \leq r \leq r_1, \quad (17)$$

and

$$p_2'(L, r) = p_4'(0, r), \quad 0 \leq r \leq r_1. \quad (18)$$

The kinematic matching condition yields,

$$\left[1 - M\lambda^n\right]^{-T} \frac{\partial p_1'}{\partial x}(0, r) = \left[1 - Mk^n\right]^{-T} \frac{\partial p_c'}{\partial x}(0, r), \quad 0 \leq r \leq r_1, \quad (19 \text{ a})$$

$$0 = \frac{1}{\tilde{\rho}} \frac{\partial p_c'}{\partial x}(0, r), \quad r_1 \leq r \leq r_2, \quad (19 \text{ b})$$

and

$$\left[1 - M\lambda^n\right]^T \frac{\partial p'_4}{\partial x}(0, r) = \left[1 - Mk^n\right]^T \frac{\partial p'_c}{\partial x}(L, r), \quad 0 \leq r \leq r_1, \quad (20 \text{ a})$$

$$0 = \frac{1}{\tilde{\rho}} \frac{\partial p'_c}{\partial x}(L, r), \quad r_1 \leq r \leq r_2. \quad (20 \text{ b})$$

Here, the wavenumbers λ and k are written in general; a distinction between the incident and reflected waves is introduced only after differentiating the general expression for pressure.

Mode matching proceeds by choosing a weighting function for each matching condition and then integrating over the cross-sectional area of the inlet/outlet pipe and the silencer chamber. Here, the incident eigenfunction in region 1 is used as the weighting function for equations (17) and (18); the incident eigenfunction in the silencer chamber is used as the weighting function for equations (19) and (20). Accordingly, substituting equations (3), (4) and (8) into the axial matching conditions, applying the weighting functions, and then integrating over the relevant cross-section, yields

$$A^n I_{11_r}^{mn} - B^n I_{1C_i}^{mn} - \tilde{C}^n e^{ik_0 k_r^n L} I_{1C_r}^{mn} = -F^0 I_{11_i}^{m0}, \quad (21)$$

$$A^n \frac{\lambda_r^n}{\left[1 - M\lambda_r^n\right]^T} I_{C1_r}^{mn} - B^n k_i^n I_{CC_i}^{mn} - \tilde{C}^n k_r^n e^{ik_0 k_r^n L} I_{CC_r}^{mn} = -F^0 \frac{\lambda_i^0}{\left[1 - M\lambda_i^0\right]^T} I_{C1_i}^{m0}, \quad (22)$$

$$B^n e^{-ik_0 k_i^n L} I_{1C_i}^{mn} + \tilde{C}^n I_{1C_r}^{mn} - D^n I_{11_i}^{mn} = 0, \quad (23)$$

$$B^n k_i^n e^{-ik_0 k_i^n L} I_{CC_i}^{mn} + \tilde{C}^n k_r^n I_{CC_r}^{mn} - D^n \frac{\lambda_i^n}{\left[1 - M\lambda_i^n\right]^T} I_{C1_i}^{mn} = 0. \quad (24)$$

Here,

$$I_{11_{i,r}}^{mn} = \int_0^{r_1} r \Phi_i^m(r) \Phi_{i,r}^n(r) dr, \quad (25)$$

$$I_{C_{1,r}}^{mn} = I_{1C_{i,r}}^{mn} = \int_0^{\eta_1} r \Psi_i^m(r) \Phi_{i,r}^n(r) dr, \quad (26)$$

$$I_{CC_{i,r}}^{mn} = \left[1 - Mk_{i,r}^n\right]^{-T} \int_0^{\eta_1} r \Psi_i^m(r) \Psi_{i,r}^n(r) dr + \tilde{\rho}^{-1} \int_{\eta_1}^{\eta_2} r \Psi_i^m(r) \Psi_{i,r}^n(r) dr, \quad (27)$$

and $\tilde{C}^n = C^n e^{-ik_0 k_r^n L}$, for a silencer of length L . These integrals are computed in Appendix B. Equations (21) to (24) assume that a plane wave is incident in region 1 (so that $F^n = 0$, for $n > 0$, and $F^0 = 1$) and that region 4 is terminated anechoically (so that $E^n = 0$, for all n). This system of equations forms a complete set of $2(N_1 + N_C)$ equations and corresponding unknowns (the modal amplitudes), where N_1 and N_C represent the number of modes at which the sums are truncated in regions 1 (or 4) and the chamber, respectively. Finally, the transmission loss (TL) for the silencer is given by

$$\text{TL} = -20 \log_{10} |D^0|, \quad (28)$$

assuming that a plane wave propagates in region 4. It is common also to express silencer performance in terms of four poles so that predictions may be integrated with other components in an exhaust system. Here, the four poles are defined by

$$\begin{bmatrix} p_1'(0) \\ u_1'(0) \end{bmatrix} = \begin{bmatrix} T_{11} & T_{12} \\ T_{21} & T_{22} \end{bmatrix} \begin{bmatrix} p_4'(0) \\ u_4'(0) \end{bmatrix}. \quad (29)$$

This gives

$$T_{11} = 2(1 + A^0)/D^0, \quad T_{12} = -Z(1 + A^0)/D^0, \quad (30 \text{ a,b})$$

and

$$T_{21} = 2(1 - A^0)/ZD^0, \quad T_{22} = -(1 - A^0)/D^0, \quad (31 \text{ a,b})$$

where $Z = \rho_0 c_0$.

III. EXPERIMENT

Experimental measurements are reported here for three straight-through circular dissipative silencers; see Table I for the silencer dimensions. The silencers, and the transmission loss measurements reported here, are identical to those studied by Kirby⁶ and so the reader is referred to Ref. 6 for a detailed description of the experimental methodology. It should be noted, however, that the impulse technique is used here for reasons of available laboratory space, and that the transmission loss measurements are valid only over a limited frequency range of approximately 150 Hz to 1500 Hz. At low frequencies, experimental errors appear because of reflections from the end of the apparatus. At high frequencies, flow noise increases and is seen to cause fluctuations in the measured data because the signal to noise ratio has dropped. This problem is exacerbated by a reduction in the sound power delivered by a rectangular pulse at higher frequencies coinciding with the frequency range in which the silencer works most effectively. It is possible that these problems may be reduced by using an alternative method, such as two-microphone method (see for example Ref. 15), and by using error analysis to suppress flow noise¹⁶. Problems with flow noise are, however, still evident in the measurements of Lee and Ih¹⁵, and obtaining accurate transmission loss predictions over a wide frequency

range when mean flow is present still represents a considerable challenge, which is reflected in the relative dearth of experimental data for dissipative silencers with mean flow in the literature.

The bulk acoustic properties of the materials in each silencer are the same as those in Ref. 6, and so the normalised propagation constant is given by

$$\tilde{\Gamma} = a_1 \xi^{-a_2} + i(1 + a_3 \xi^{-a_4}), \quad (32)$$

and the normalised complex density by

$$\tilde{\rho} = -\tilde{\Gamma}[a_5 \xi^{-a_6} + i(1 + a_7 \xi^{-a_8})]. \quad (33)$$

Here, the constants $a_1 \dots a_8$ are Delany and Bazley coefficients that are given for each material in Table II; ξ is a non-dimensional frequency parameter given by $\xi = \rho_0 f / \Theta$, where Θ is the material flow resistivity (see Table II). A low frequency correction, discussed in detail by Kirby^{6,9} is also used here, which requires the material porosity Ω , the “steady flow” tortuosity q_0^2 , and a so-called transition value for ξ , known as ξ_0 ; values for these parameters are also listed in Table II.

Values for the impedance of the perforated screen depend on experimental measurements. Kirby^{6,9} used the semi-empirical model proposed by Kirby and Cummings¹² to quantify the impedance of a perforated screen under grazing flow. These results have since been reviewed by other authors and it is apparent that values for the impedance may depend on the degree to which the viscous boundary layer in the test rig has developed by the time the flow reaches a perforation. The impedance data proposed by Kirby and Cummings was measured on the same

test rig as the transmission loss predictions presented here, and so it appears sensible to retain these results in this current study. However, it is interesting also to review how other measured impedance data affects the transmission loss predictions and so the data of Lee and Ih¹⁵ will also be reviewed here. Kirby and Cummings¹² also measured the effect of a fibrous material on the impedance of the perforated screen and suggested adding a correction, based on replacing the density of air with the effective complex density of the fibrous material, to the expression for the impedance. Lee *et al.*¹⁷ recently investigated this correction by using detailed experimental measurements without mean flow, and concluded that this is indeed capable of capturing the effect of the absorbing material on the perforate impedance. Accordingly, this correction is retained here, although Denia *et al.*¹⁸ suggest modifying this correction by introducing the parameter $F(\sigma)$, where

$$F(\sigma) = 1 - 1.06\sigma^{0.5} + 0.17\sigma^{1.5}. \quad (34)$$

Here, σ is the open area porosity of the perforated screen and the normalised impedance ζ is then given as,

$$\zeta = [\zeta' + i0.425k_0d(\tilde{\rho} - 1)F(\sigma)]/\sigma, \quad (35)$$

where d is the diameter of the hole and ζ' is the orifice impedance measured in the absence of a porous material. In view of the good correlation between prediction and experiment observed by Denia *et al.*¹⁸, $F(\sigma)$ will be retained here and all transmission loss calculations that include a perforate will use equation (35). Values for ζ' measured by Kirby and Cummings¹² (see also Refs. 6 and 9) and Lee and Ih [15] will be used here with a perforate screen that has a thickness of 1 mm, a hole diameter of 3.5 mm and an open area porosity of 26.3%.

IV. RESULTS AND DISCUSSION

A. Axial continuity condition.

In this section, changing the axial kinematic matching condition from continuity of velocity (the method used by Cummings and Chang⁴) to continuity of displacement is investigated. In principle, both conditions should deliver identical predictions when used in a mode matching scheme applied to the silencers studies here, even when mean flow is present; however, the results presented will demonstrate that problems arise with Cummings and Chang's method. In Ref. 9 it is argued that mode matching depends on finding a convergent system of equations that form a transfer matrix, \mathbf{S} , whose elements S_{ij} decay rapidly with increasing i, j . Moreover, without such a property, one cannot guarantee that the final solution will reflect the physics of the problem. When mean flow is neglected, equation (27) provides an orthogonality relation that guarantees a convergent system of equations; however, when mean flow is present the silencer eigenfunctions are not orthogonal and equation (27) no longer provides a true orthogonality relation. Accordingly, in the absence of an orthogonality relation when mean flow is present, one must be careful first to establish a convergent system of equations before one can be sure the solution reflects the physics of the problem. To investigate this issue for dissipative silencers, a number of different geometries are examined here. First, in Fig. 2 convergence is examined for the silencer studied by Xu et al.¹⁰ For this silencer, the inner radius of the porous material is coincident with the radius of the inlet/outlet pipe, the excitation frequency is 40 Hz, the mean flow Mach number is 0.15 and a perforated screen is omitted. Transmission loss predictions using the new approach (with $T = 2$) are compared with Cummings and Chang's method⁴ and

the finite element method⁸ (with 1545 degrees of freedom); for the latter two models internal mean flow is neglected. A problem with convergence for Cummings and Chang's method is clearly evident in Fig. 2, and non-physical predictions occur when higher order modes are added. In contrast, the new method is seen to converge smoothly towards the (benchmark) finite element predictions. In Fig. 3, transmission loss predictions for Xu et al.'s silencer are presented over a range of frequencies and the new mode matching predictions (with $N_c = 8$) compare very well with the finite element method, especially at low frequencies. Conversely, problems with Cummings and Chang's method are obvious in the form of predictions that are too low (in some instances negative) at low frequencies, although better agreement with the finite element predictions is observed at higher frequencies.

The problems observed with Cummings and Chang's method in Figs. 2 and 3 are thought to be caused by the absence of a convergent system of equations when different axial and radial kinematic matching conditions are applied at the silencer edges (at $r = r_1$, for $x = 0$ and $x = L$). On enforcing the same kinematic boundary condition, it is evident that predictions now agree well with finite elements and this is thought to be because the new boundary condition delivers a transfer matrix, \mathbf{S} , whose elements \mathbf{S}_{ij} decay rapidly with increasing i, j . Further evidence to support this is provided in Fig. 4, which compares transmission loss predictions for Cummings and Chang's silencer (for $M = 0.196$, perforated screen and internal mean flow omitted). Here, Cummings and Chang's method is again seen to provide predictions that are too low over an important part of the frequency range, whereas the new method agrees well with the finite element predictions. Also included in this figure are point collocation predictions obtained using the method of Kirby⁹. The point collocation method is a numerical version of mode matching

and the method presented in Ref. 9 is based on the same axial kinematic matching condition used by Cummings and Chang. Accordingly, one would expect the two methods to provide similar predictions and in Fig. 4 this is seen to be the case, even at low frequencies. Here, the failure of Kirby's method at low frequencies is thought to be for the same reasons as that seen for Cummings and Chang's method, namely the failure to deliver a convergent system of equations. This does not, however, explain why the predictions presented by Kirby 9 provided good agreement with experimental data and why agreement improves at higher frequencies in Figs. 3 and 4. To investigate this further, point collocation predictions are presented in Fig. 5 for silencer A ($M = 0.15, u_* = 2.56 \text{ m/s}$), and these are shown to agree well with predictions generated using the new method ($T = 2$), even at low frequencies (note that the point collocation predictions overlay those obtained using Cummings and Chang's method). This good agreement is thought to be because Cummings and Chang's transfer matrix is sufficiently convergent to provide sensible predictions for those materials with a high flow resistivity. Furthermore, similar convergent conditions also exist for the silencer transfer matrix when materials of low flow resistivity are present, but only at high frequencies (see Figs. 3 and 4). Similar behaviour is observed, as one would expect, for the point collocation results in Figs. 4 and 5, and this indicates that the reason for the good agreement between prediction and measurement is the high material flow resistivity used in the silencers studied by Kirby 9. It appears, therefore, that in order properly to reflect the physics of the problem over a wide range of parameters, a true orthogonality relation is not required provided that one carefully chooses the kinematic matching conditions in order to realise a convergent system of equations. Accordingly, when mean flow is present, the results presented here indicate that if continuity of displacement is used as a radial boundary condition, then the correct axial continuity condition is also displacement. But, if the

radial boundary condition changes, say to continuity of velocity, then the axial boundary condition must also change. This conclusion is based on numerous numerical experiments, although only a sample is shown in this paper. In the current study, equality of the kinematic matching conditions is enforced by the use of the constant T , and all further transmission loss predictions presented here will use this new approach.

B. Boundary conditions for the perforated screen.

The boundary conditions for the perforated screen are defined by a pressure condition, equation (14), and a kinematic continuity condition, equation (13). The constant T allows for the alteration of the kinematic continuity condition and in Figs. 5-7 mode matching predictions are presented (with $N_1 = 1$, $N_c = 8$) for values of T of 1, 1.5, and 2, for silencers A, B, and C respectively. Here, $M = 0.15$ and a perforated screen with the impedance specified by Kirby and Cummings¹² is used in equation (35) (with $u_* = 2.56$ m/s). In Figs. 5-7 it is evident that changing the axial and radial kinematic boundary conditions has a significant effect on transmission loss: in each case, predictions for continuity of velocity ($T = 1$) are higher than those for continuity of displacement ($T = 2$), and not surprisingly predictions for $T = 1.5$ bisect these two extremes. For silencers A and C, continuity of displacement provides good agreement with measurement, although for silencer B some under prediction is evident. In contrast, continuity of velocity consistently over predicts the transmission loss for all three silencers. It is evident that by altering the value for T improvements in the correlation between prediction and experiment may be obtained for silencer B; however, there does not appear to be a consistent value for T that provides good agreement for all silencers. Thus, in view of these results, and the successful use of continuity of displacement in other dissipative silencer models that assume

uniform mean flow, it appears prudent here to retain continuity of displacement as the kinematic boundary condition. Accordingly, this condition is used in the following section, which reviews two different impedance models. We note, however, that more supporting evidence in the form of further transmission loss measurements is required before one can be certain of the correct boundary conditions for the perforated screen.

C. Predicted and measured transmission loss.

This section presents comparisons between transmission loss measurements and predictions found using the impedance data for a perforated screen measured by Kirby and Cummings¹², and Lee and Ih¹⁵. In both cases, a Mach number of $M = 0.15$ is present (with $u_* = 2.56$ m/s for Ref. [12]), $T = 2$, $N_1 = 1$, and $N_c = 8$. In Fig. 8 a comparison is presented for silencer A, which has a perforated screen porosity of $\sigma = 0.263$. This porosity lies outside Lee and Ih's suggested limits of $0.0279 \leq \sigma \leq 0.223$; however, the difference here is small and, as the influence of the perforated screen will reduce at higher porosities, any inaccuracies associated with this extrapolation are likely to have a negligible effect on the transmission loss predictions. In general, good agreement between prediction and experiment is observed in Fig. 8, and it is noticeable that the two impedance models give largely similar predictions over the frequency range shown. The effect of the perforated screen is clearly evident, especially at higher frequencies, and for the silencers studied here an improvement in the agreement between prediction and experiment is observed when a perforated screen is included. It is, however, difficult to arrive at conclusions regarding the most appropriate impedance model, especially as one could argue that the data here is biased towards the method of Kirby and Cummings since the transmission loss measurements were obtained under the same mean flow conditions as the

impedance measurements. Further observations regarding an appropriate choice for impedance data awaits additional silencer measurements, especially measurements that are reliable at much higher frequencies. Nevertheless, the new mode matching approach is demonstrated here to work well, and it is noticeable that there is no under prediction of transmission loss at low frequencies, further supporting the change in the axial boundary condition.

V. CONCLUSIONS

When mean flow is added to the central airway of a straight-through circular dissipative silencer, the analytic mode matching schemes developed without flow may readily be extended to include flow. The mode matching scheme presented here uses the silencer eigenfunctions as weighting functions and good agreement is observed between the mode matching predictions, experimental data and benchmark finite element calculations. The main result of this study is that if mean flow and higher order modes are included in the matching scheme, the axial kinematic continuity condition must be the same as the radial kinematic boundary condition chosen for the interface between the airway and the material (regardless of whether a perforated screen is present or not). That is, if continuity of pressure and displacement are chosen for the radial boundary conditions then the axial matching conditions should also be continuity of pressure and displacement, rather than pressure and velocity as previously thought. In this study, equality for the axial and radial kinematic boundary conditions is enforced using a constant T , where using $T = 2$ enforces continuity of displacement and $T = 1$ continuity of velocity. On adding a perforated screen, the appropriate radial kinematic boundary condition is reviewed by varying T . Here, good

agreement between prediction and experiment is observed using continuity of displacement, whereas the transmission loss tends to be over predicted when using continuity of velocity. Finally, two different sets of impedance data for the perforated screen were reviewed and it is demonstrated that similar transmission loss predictions are obtained at low to medium frequencies when using the data of Kirby and Cummings¹² and Lee and Ih.¹⁵

APPENDIX A: ROOT FINDING

The roots of equation (15) provide the incident and reflected axial wavenumbers in the silencer chamber. There are numerous methods available for finding these roots, although in the design of dissipative silencers three methods have found favour: the Newton Raphson method², Muller's method¹⁹, and the Secant method¹¹. Each method has its own advantages and disadvantages; however, a problem common to all root finding techniques is the possibility of missing roots. This happens because each method depends on inputting an initial guess, or guesses, and then iterating towards the desired root. If the root is complex (as it is for dissipative silencers) one cannot guarantee that the initial guess is close enough to locate a desired root. This problem is further exacerbated when attempting to track roots over a frequency sweep, as it can be readily shown that roots may jump position in the complex plane. Selamet *et al.*¹¹ adopt the Secant method in order to find the roots of an eigenequation that is similar (but without mean flow) to equation (15) and use initial guesses based on limiting values at high frequencies. This procedure was found to succeed for the silencer geometries and material parameters chosen in their study, but in general an iterative method does not, and cannot, guarantee to find all desired roots over a specified region in the complex plane unless one first uses the Argument Principle²⁰ to see if any roots have been missed, and then laboriously searches smaller segments of the complex plane, again with the aid of the Argument Principle, in order to locate a missing root. This procedure must be repeated for every root and every time a parameter, such as frequency, is changed. This issue is discussed in more detail by Lawrie and Kirby²¹ who avoid root finding altogether, although this method depends on writing an orthogonality relation for the system and so is not currently applicable when mean flow is present. The salient point, however, is that all

root finding techniques suffer from the problem of missing roots and one must be wary of this when using an analytic mode matching scheme such as the one reported here. The authors' preference is to use the Argument Principle as a check to make sure all desired roots have been found, but if roots have been missed then to refine the initial guess(es) (for example, by increasing the number of guesses) rather than laboriously searching the complex plane for the missing root. A further complication in the current analysis is the presence of mean flow. Here, the authors have found that it is harder to track and locate roots when mean flow is present. The authors' preferred method for finding roots is the Newton Raphson method, as this method converges faster than the secant method and requires only one initial guess, unlike Muller's method. The Newton Raphson method does, however, require the derivative of the governing eigenequation to be found. To facilitate this, equation (15) is recast here to give

$$G(k) = \frac{\beta}{\alpha} [1 - Mk]^T (b_1 - b_4) + \frac{i\zeta\beta}{k_0} (h_1 - h_2) - \tilde{\rho}(h_3 - h_6). \quad (\text{A1})$$

The derivative is then given by

$$G'(k) = G_1(k) - G_2(k), \quad (\text{A2})$$

where

$$G_1(k) = \frac{k_0^2}{\alpha^3 \beta} [1 - Mk]^T (g_{11} - g_{12}) - \frac{\beta}{\alpha} TM [1 - Mk]^{T-1} (b_1 - b_4), \quad (\text{A3})$$

and

$$G_2(k) = \frac{i\zeta k_0}{\alpha^2 \beta} (g_{21} - g_{22}) + \frac{\tilde{\rho} k_0^2}{\alpha^2 \beta^2} (g_{31} - g_{32}). \quad (\text{A4})$$

Here

$$g_{11} = \alpha^2 k b_1 + s(b_1 + \alpha r_1 h_1) - \alpha^2 \beta k (r_1 b_2 + r_2 b_3), \quad (\text{A5})$$

$$g_{12} = \alpha^2 k b_4 + s(b_4 + \alpha r_1 h_2) - \alpha^2 \beta k (r_2 b_5 + r_1 b_6), \quad (\text{A6})$$

$$g_{21} = -\alpha^2 k h_1 + s(\alpha r_1 b_1 - h_1) + \alpha^2 \beta k (r_1 h_3 + r_2 h_4), \quad (\text{A7})$$

$$g_{22} = -\alpha^2 k h_2 + s(\alpha r_1 b_4 - h_2) + \alpha^2 \beta k (r_2 h_5 + r_1 h_6), \quad (\text{A8})$$

$$g_{31} = \alpha^2 k (\beta [r_1 h_1 - r_2 h_7] + h_3) - s(\alpha r_1 b_2 - h_3), \quad (\text{A9})$$

$$g_{32} = \alpha^2 k (\beta [r_1 h_2 - r_2 h_8] + h_6) - s(\alpha r_1 b_6 - h_6); \quad (\text{A10})$$

and

$$s = \beta^2 [M + (1 - M^2)k], \quad (\text{A11})$$

$$b_1 = J_0(\alpha r_1) J_1(\beta r_1) Y_1(\beta r_2), \quad (\text{A12})$$

$$b_2 = J_0(\alpha r_1) J_0(\beta r_1) Y_1(\beta r_2), \quad (\text{A13})$$

$$b_3 = J_0(\alpha r_1) J_1(\beta r_1) Y_0(\beta r_2), \quad (\text{A14})$$

$$b_4 = J_0(\alpha r_1) J_1(\beta r_2) Y_1(\beta r_1), \quad (\text{A15})$$

$$b_5 = J_0(\alpha r_1) J_0(\beta r_2) Y_1(\beta r_1), \quad (\text{A16})$$

$$b_6 = J_0(\alpha r_1) J_1(\beta r_2) Y_0(\beta r_1), \quad (\text{A17})$$

$$h_1 = J_1(\alpha r_1) J_1(\beta r_1) Y_1(\beta r_2), \quad (\text{A18})$$

$$h_2 = J_1(\alpha r_1) J_1(\beta r_2) Y_1(\beta r_1), \quad (\text{A19})$$

$$h_3 = J_1(\alpha r_1) J_0(\beta r_1) Y_1(\beta r_2), \quad (\text{A20})$$

$$h_4 = J_1(\alpha r_1) J_1(\beta r_1) Y_0(\beta r_2), \quad (\text{A21})$$

$$h_5 = J_1(\alpha r_1) J_0(\beta r_2) Y_1(\beta r_1), \quad (\text{A22})$$

$$h_6 = J_1(\alpha r_1) J_1(\beta r_2) Y_0(\beta r_1), \quad (\text{A23})$$

$$h_7 = J_1(\alpha r_1) J_0(\beta r_1) Y_0(\beta r_2), \quad (\text{A24})$$

$$h_8 = J_1(\alpha r_1) J_0(\beta r_2) Y_0(\beta r_1). \quad (\text{A25})$$

Roots of equation (A1) are found by supplying a number of initial guesses to the Newton Raphson scheme in order to locate N eigenmodes for the incident or reflected wave. The methodology used here begins at a low frequency, say at 20 Hz, and starts with two initial guesses based on the low frequency model of Kirby⁶. Then $8N$ further guesses are added, and these are:

$$k_{i,r}^n = \left\{ -M \mp \sqrt{1 - (1 - M^2) \left\{ \frac{a_0^n}{k_0 r_1} \right\}^2} \right\} / (1 - M^2), \quad (\text{A26})$$

$$k_{i,r}^n = \left\{ -M \mp \sqrt{1 - (1 - M^2) \left\{ \frac{a_0^n}{k_0 r_2} \right\}^2} \right\} / (1 - M^2), \quad (\text{A27})$$

$$k_{i,r}^n = \pm \sqrt{-\tilde{\Gamma}^2 + \left\{ \frac{a_0^n}{k_0 r_1} \right\}^2}, \quad (\text{A28})$$

$$k_{i,r}^n = \pm \sqrt{-\tilde{\Gamma}^2 + \left\{ \frac{a_0^n}{k_0 r_2} \right\}^2}, \quad (\text{A29})$$

$$k_{i,r}^n = \pm \sqrt{-\tilde{\Gamma}^2 + \left\{ \frac{b_0^n}{k_0 r_1} \right\}^2}, \quad (\text{A30})$$

$$k_{i,r}^n = \pm \sqrt{-\tilde{\Gamma}^2 + \left\{ \frac{b_0^n}{k_0 r_2} \right\}^2}, \quad (\text{A31})$$

$$k_{i,r}^n = \pm \left(2M - i \frac{b_0^n}{k_0 r_1} \right), \quad (\text{A32})$$

$$k_{i,r}^n = \pm \left(2M - i \frac{b_0^n}{k_0 r_2} \right). \quad (\text{A33})$$

Here, a_0^n and b_0^n are solutions of $J_0(a_0) = 0$ and $Y_0(b_0) = 0$ respectively. After finding all the required roots (N incident, N reflected) at the starting frequency, the frequency is then

incremented upwards, say by 10 Hz, and those roots found at the starting frequency are then used as the initial guesses for the following frequency. Crucially, however, the additional $8N$ guesses previously mentioned are also used, thus increasing the number of initial guesses to $9N$. For frequencies that follow, those N roots found at the previous frequency, along with the $8N$ guesses in equations (A26) to (A33), are used as initial guesses. Accordingly, this approach adopts the tactic of using a large number of initial guesses to provide a high probability that all required roots are found. Obviously, this requires a method that converges quickly, hence the use of Newton Raphson, and repeated roots must also be filtered out. The authors do not claim that this approach represents an optimum, in terms of number and/or value of the guesses chosen; instead, this approach has been arrived at using trial and error for a large number of silencer configurations (including differing mean flow Mach numbers and materials) and is deliberately over specified in order to give the best possible chance of locating all required roots. On locating N incident and reflected axial wavenumbers $k_{x_{i,r}}$, these are then sorted in ascending order of the imaginary part for use in the mode matching scheme that follows.

APPENDIX B: EIGENFUNCTION INTEGRALS

The integrals defined in equations (25) to (27) are given by,

$$I_{1i,r}^{mn} = \begin{cases} 0 & m \neq n \\ \frac{r_1^2}{2} J_0(\gamma_i^m r_1) J_0(\gamma_i^m r_1) & m = n \end{cases}, \quad (\text{B1})$$

$$I_{1C_i,r}^{mn} = \begin{cases} \frac{r_1}{(\alpha_{i,r}^n)^2 - (\gamma_i^n)^2} \left[\alpha_{i,r}^n J_1(\alpha_{i,r}^n r_1) J_0(\gamma_i^m r_1) \right] & (\alpha_{i,r}^n)^2 \neq (\gamma_i^m)^2 \\ \frac{r_1^2}{2} J_0(\alpha_{i,r}^n r_1) J_0(\gamma_i^m r_1) & (\alpha_{i,r}^n)^2 = (\gamma_i^m)^2 \end{cases}. \quad (\text{B2})$$

For $m = n$,

$$I_{CC_i}^{mn} = \frac{r_1^2}{2} \frac{[J_0^2(\alpha_i^n r_1) + J_1^2(\alpha_i^n r_1)]}{[1 - Mk_i^n]^T} + \frac{\tilde{\rho} r_2^2}{2} \frac{(\alpha_i^n)^2}{(\beta_i^n)^2} \frac{J_1^2(\alpha_i^n r_1)}{[1 - Mk_i^n]^{2T}} \left\{ t_3^n - \frac{r_1^2}{r_2^2} t_4^n \right\}, \quad (\text{B3})$$

and

$$I_{CC_r}^{mn} = \begin{cases} I_{CC_i}^{mn} & M = 0 \\ \frac{t_{1,r}^{mn} r_1}{[1 - Mk_r^n]^T} - \frac{t_{2,r}^{mn} r_1}{[(\beta_r^n)^2 - (\beta_i^m)^2]} & M > 0 \end{cases}. \quad (\text{B4})$$

For $m \neq n$,

$$I_{CC_{i,r}}^{mn} = \frac{t_{1,r}^{mn} r_1}{[1 - Mk_{i,r}^n]^T} - \frac{t_{2,r}^{mn} r_1}{[(\beta_{i,r}^n)^2 - (\beta_i^m)^2]}. \quad (\text{B5})$$

Here,

$$t_{i,r}^{mn} = \left[\alpha_{i,r}^n J_1(\alpha_{i,r}^n r_1) J_0(\alpha_i^m r_1) - \alpha_i^m J_0(\alpha_{i,r}^n r_1) J_1(\alpha_i^m r_1) \right] / [(\alpha_{i,r}^n)^2 - (\alpha_i^m)^2], \quad (\text{B6})$$

$$t_{2,i,r}^{mn} = \frac{\alpha_{i,r}^n J_1(\alpha_{i,r}^n r_1) J_0(\alpha_i^m r_1)}{[1 - Mk_{i,r}^n]^T} - \frac{\alpha_i^m J_0(\alpha_{i,r}^n r_1) J_1(\alpha_i^m r_1)}{[1 - Mk_i^n]^T}, \quad (\text{B7})$$

$$t_3^n = \frac{[J_0(\beta_i^n r_2) Y_1(\beta_i^n r_2) - J_1(\beta_i^n r_2) Y_0(\beta_i^n r_2)]^2}{[J_1(\beta_i^n r_1) Y_1(\beta_i^n r_2) - J_1(\beta_i^n r_2) Y_1(\beta_i^n r_1)]^2}, \quad (\text{B8})$$

$$t_4^n = 1 + \frac{[J_0(\beta_i^n r_1) Y_1(\beta_i^n r_2) - J_1(\beta_i^n r_2) Y_0(\beta_i^n r_1)]^2}{[J_1(\beta_i^n r_1) Y_1(\beta_i^n r_2) - J_1(\beta_i^n r_2) Y_1(\beta_i^n r_1)]^2}. \quad (\text{B9})$$

REFERENCES

1. B. Nilsson and O. Brander, "The propagation of sound in cylindrical ducts with mean flow and bulk reacting lining: I. Modes in an infinite duct," *J. Inst. Maths Appl.* **26**, 269-298 (1980).
2. A. Cummings and I.-J. Chang, "Internal mean flow effects on the characteristics of bulk-reacting liners in circular ducts," *Acustica* **64**, 170-178 (1987).
3. R.J. Astley and A. Cummings, "A finite element scheme for attenuation in ducts lined with porous material: comparison with experiment," *J. Sound Vib.* **116**, 239-263 (1987).
4. A. Cummings and I.-J. Chang, "Sound attenuation of a finite length dissipative flow duct silencer with internal mean flow in the absorbent," *J. Sound Vib.* **127**, 1-17 (1988).
5. K.S. Peat, "A transfer matrix for an absorption silencer element," *J. Sound Vib.* **146**, 353-360 (1991).
6. R. Kirby, "Simplified techniques for predicting the transmission loss of a circular dissipative silencer," *J. Sound Vib.* **243**, 403-426 (2001).
7. S.N. Panigrahi and M.L. Munjal, "Comparison of various methods for analyzing lined circular ducts," *J. Sound Vib.* **285**, 905-923 (2005).
8. K.S. Peat and K.L. Rathi, "A finite element analysis of the convected acoustic wave motion in dissipative silencers," *J. Sound Vib.* **184**, 527-545 (1995).
9. R. Kirby, "Transmission loss predictions for dissipative silencers of arbitrary cross section in the presence of mean flow," *J. Acoust. Soc. Am.* **114**, 200-209 (2003).
10. M.B. Xu, A. Selamet, I.-J. Lee and N.T. Huff, "Sound attenuation in dissipative expansion chambers," *J. Sound Vib.* **272**, 1125-1133 (2004).

11. A. Selamet, M.B. Xu, I.-J. Lee and N.T. Huff, "Analytical approach for sound attenuation in perforated dissipative silencers," *J. Acoust. Soc. Am.* **115**, 2091-2099 (2004).
12. R. Kirby and A. Cummings, "The impedance of perforated plates subjected to grazing mean flow and backed by porous media," *J. Sound Vib.* **217**, 619-636 (1988).
13. Y. Aurégan and M. Leroux, "Failures in the discrete models for flow duct with perforations: an experimental investigation," *J. Sound Vib.* **265**, 109-121 (2003).
14. E. Dokumaci, "Effect of sheared grazing mean flow on acoustic transmission in perforated pipe mufflers," *J. Sound Vib.* **283**, 645-663 (2005).
15. S.-H. Lee and J.-G. Ih, "Empirical model of the acoustic impedance of a circular orifice in grazing mean flow," *J. Acoust. Soc. Am.* **114**, 98-113 (2003).
16. M. Åbom and H. Bodén, "Error analysis of two-microphone measurements in ducts with flow," *J. Acoust. Soc. Am.* **83**, 2429-2438 (1988).
17. I. Lee, A. Selamet and N.T. Huff, "Impact of perforation impedance on the transmission loss of reactive and dissipative silencers," *J. Acoust. Soc. Am.* **120**, 3706-3713 (2006).
18. F.D. Denia, A. Selamet, F.J. Fuenmayor and R. Kirby, "Acoustic attenuation performance of perforated dissipative mufflers with empty inlet/outlet extensions," *J. Sound Vib.* **302**, 1000-1017 (2007).
19. A. Cummings and N. Sormaz, "Acoustic attenuation in dissipative splitter silencers containing mean fluid flow," *J. Sound Vib.* **168**, 209-227 (1993).
20. R. Kirby and J.B. Lawrie, "A point collocation approach to modelling large dissipative silencers," *J. Sound Vib.* **286**, 313-339 (2005).
21. J.B. Lawrie and R. Kirby, "Mode matching without root finding: Application to a dissipative silencer," *J. Acoust. Soc. Am.* **119**, 2050-2061 (2006).

Table I. Data for silencers.			
Silencer	Length L (mm)	Diameter $2 \times r_2$ (mm)	Absorbent
A	315	152.4	E glass
B	330	203.2	E glass
C	450	152.4	A glass

Table II. Values of material constants.		
Constant	E glass	A glass
a_1	0.2202	0.2251
a_2	-0.5850	-0.5827
a_3	0.2010	0.1443
a_4	-0.5829	-0.7088
a_5	0.0954	0.0924
a_6	-0.6687	-0.7177
a_7	0.1689	0.1457
a_8	-0.5707	-0.5951
Θ (MKS rayl/m)	30716	5976
Ω	0.952	0.952
q_0^2	5.49	3.77
ξ_0	0.005	0.025

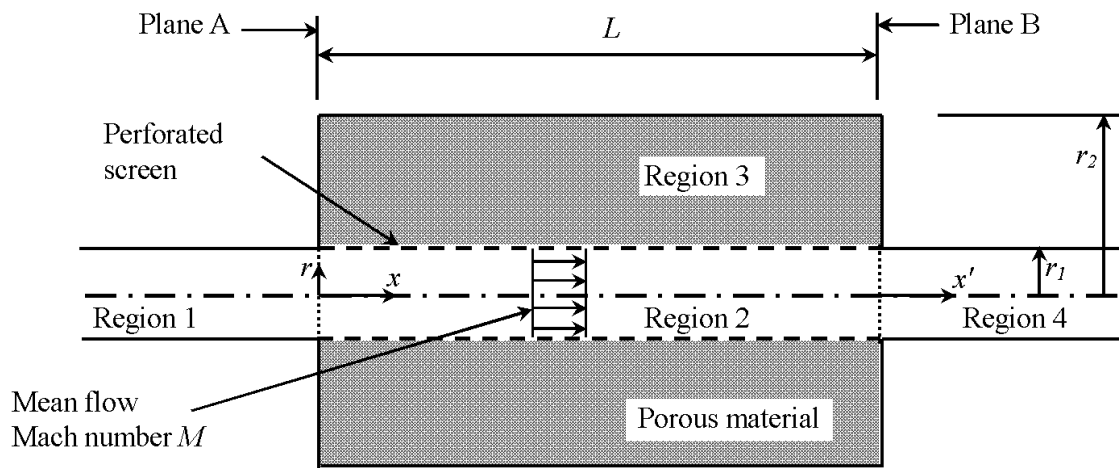


Figure 1. Geometry of silencer.

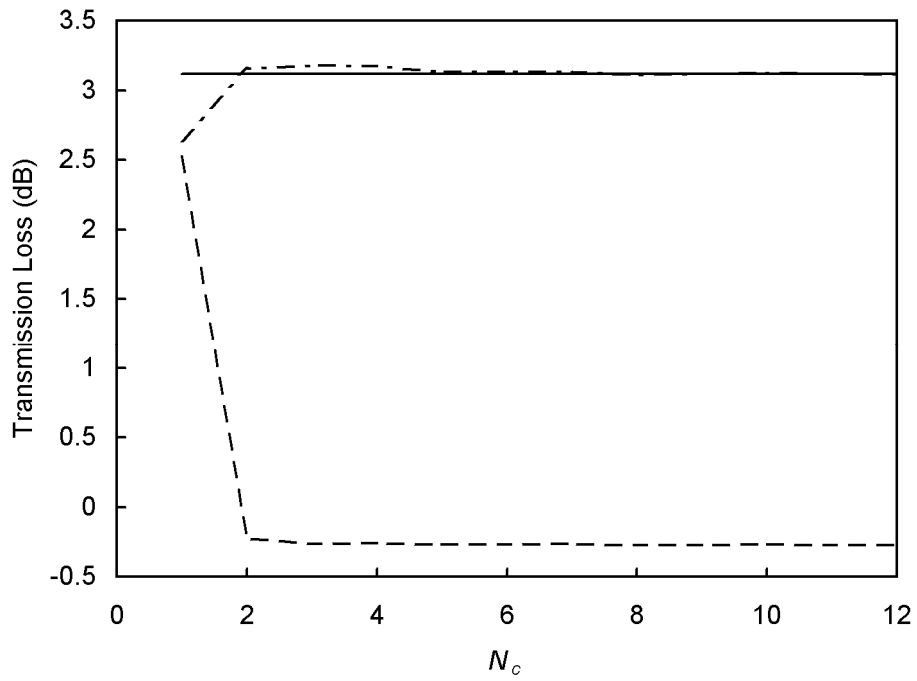


Figure 2. Predicted transmission loss for Xu *et al.* [10] silencer, for $F = 40$ Hz and $M = 0.15$ ($N_1 = 1$): ———, finite element method [8]; — — —, Cummings and Chang's method [4]; — - - - —, current method with $T = 2$.

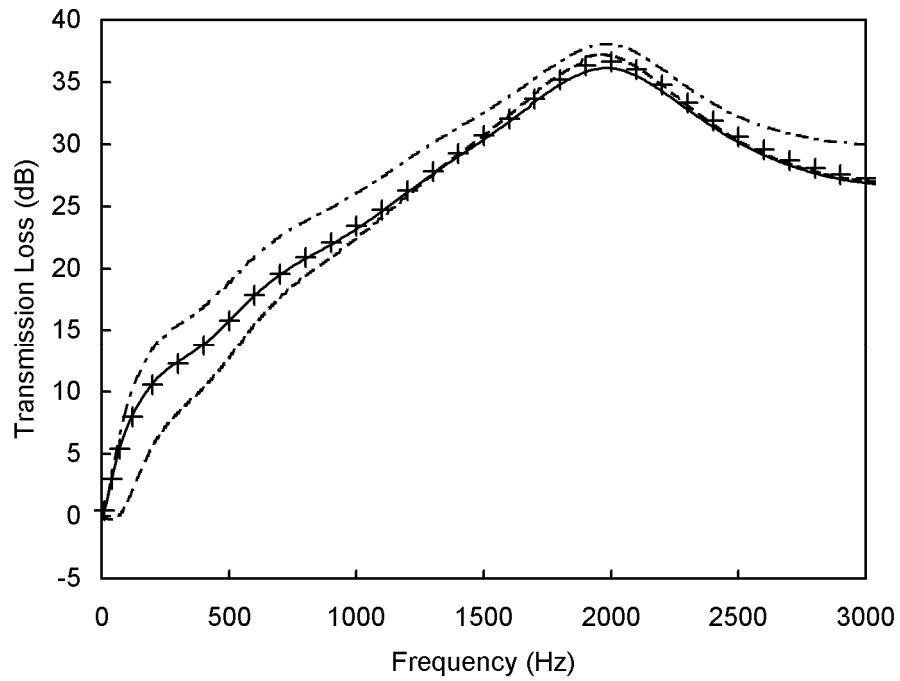


Figure 3. Predicted transmission loss for Xu *et al.* [10] silencer: + , finite element method [8], $M = 0.15$; ———, current method, $M = 0.15$; — — — , Cummings and Chang's method [4], $M = 0.15$; — - — - — , current method $M = 0$.

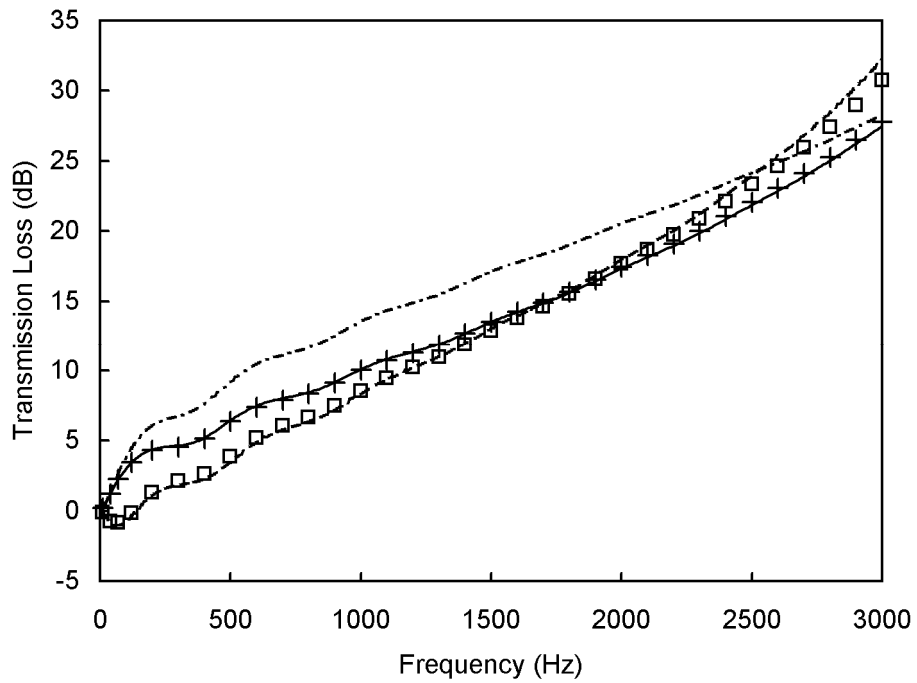


Figure 4. Predicted transmission loss for Cummings and Chang's [4] silencer (with no internal flow): +, finite element method [8], $M = 0.196$; ———, current method, $M = 0.196$; — — — —, Cummings and Chang's method [4], $M = 0.196$; — - — - —, current method $M = 0$; □, point collocation method [9], $M = 0.196$.

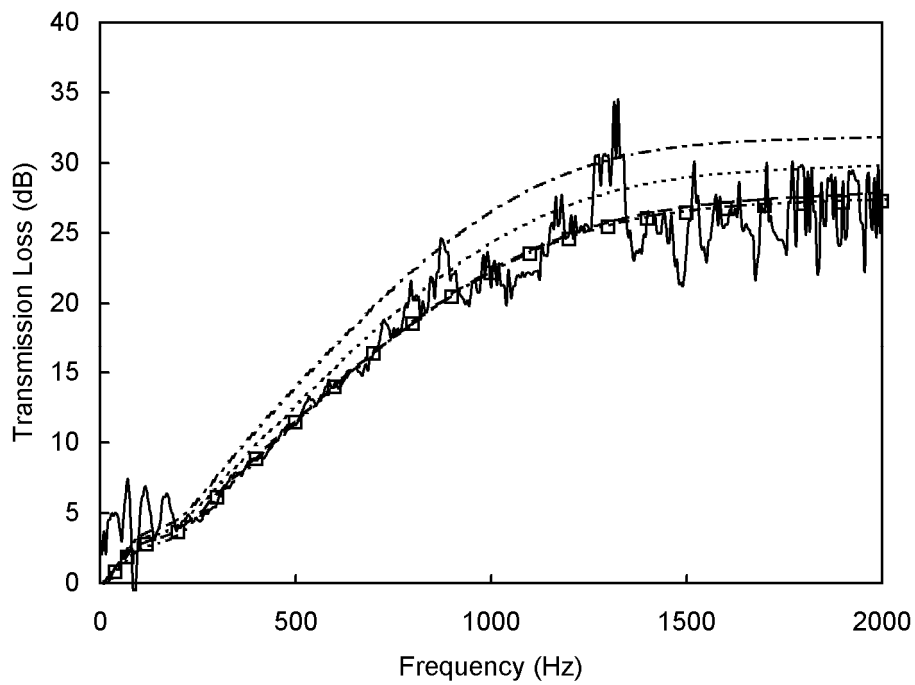


Figure 5. Predicted and measured transmission loss for silencer A, with $M = 0.15$: ——— experiment; — — —, prediction with $T = 2$; - - - - -, prediction with $T = 1.5$; — - - - —, prediction with $T = 1$; □, point collocation [9]; — - - — - - —, Cummings and Chang method [4].

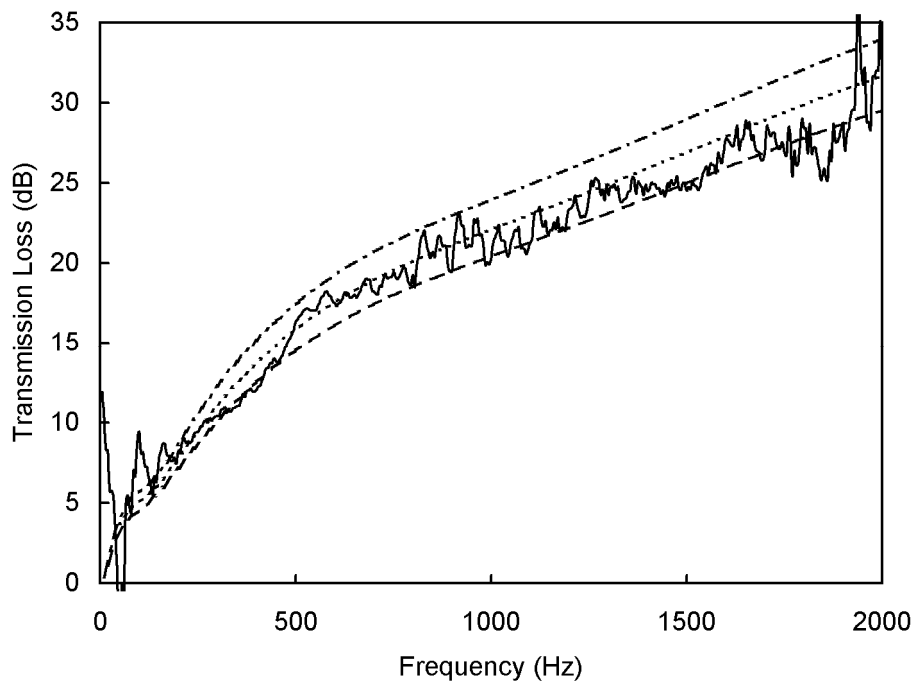


Figure 6. Predicted and measured transmission loss for silencer B, with $M = 0.15$: ——— experiment; — — —, prediction with $T = 2$; - - - - -, prediction with $T = 1.5$; — - - - —, prediction with $T = 1$.

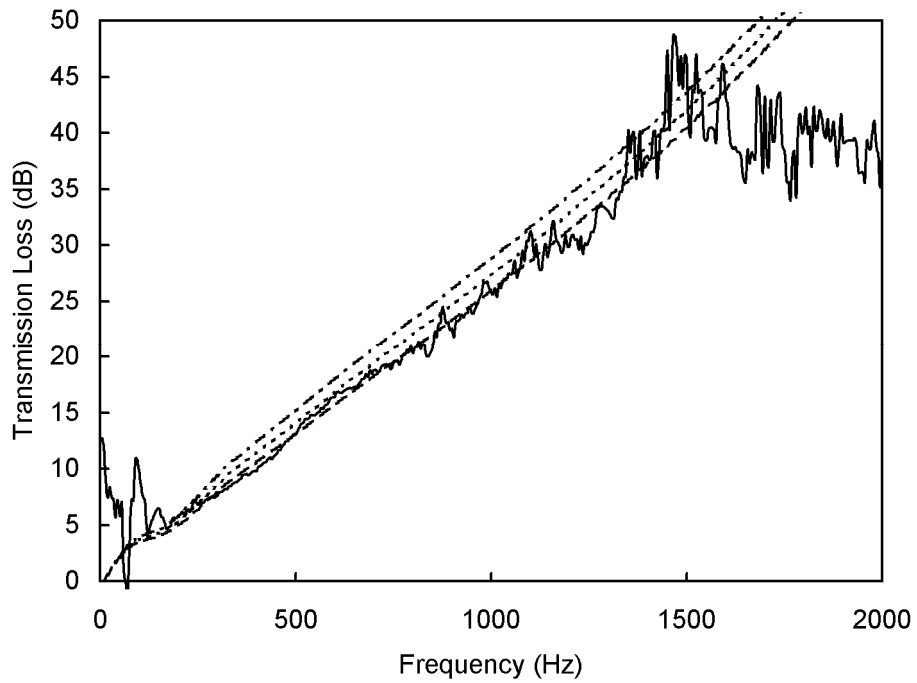


Figure 7. Predicted and measured transmission loss for silencer C, with $M = 0.15$: ——— experiment; — — —, prediction with $T = 2$; ·····, prediction with $T = 1.5$; — - - - —, prediction with $T = 1$.

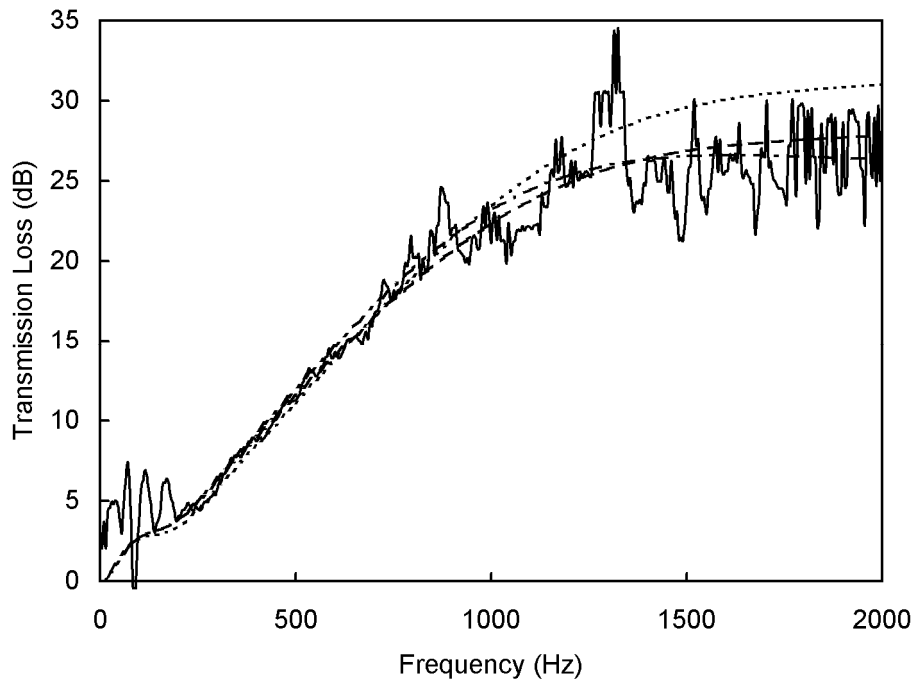


Figure 8. Predicted and measured transmission loss for silencer A, with $M = 0.15$: ——— experiment; — — —, predictions using Kirby and Cummings' perforate data [12]; — - — - —, predictions using Lee and Ih's perforate data [15]; - - - - -, prediction with no perforated screen;